

Research Paper

First-in-human uPAR PET: Imaging of Cancer Aggressiveness

Morten Persson^{1#}, Dorthe Skovgaard^{1,2#}, Malene Brandt-Larsen¹, Camilla Christensen¹, Jacob Madsen¹, Carsten H. Nielsen¹, Tine Thurison³, Thomas Levin Klausen¹, Søren Holm¹, Annika Loft¹, Anne Kiil Berthelsen¹, Michael Ploug³, Helle Pappot⁴, Klaus Brasso⁵, Niels Kroman⁶, Liselotte Højgaard¹, Andreas Kjaer¹✉

1. Department of Clinical Physiology, Nuclear Medicine & PET and Cluster for Molecular Imaging, Rigshospitalet and University of Copenhagen, Denmark.
2. Department of Physiology and Nuclear Medicine, University hospital of Copenhagen, Gentofte, Denmark
3. Finsen Laboratory, Rigshospitalet, Biotech Research & Innovation Centre, University of Copenhagen, Copenhagen, Denmark
4. Department of Oncology, Finsen Centre, Rigshospitalet, Copenhagen, Denmark.
5. Copenhagen Prostate Cancer Center, Department of Urology, Abdominal Centre, Rigshospitalet, Copenhagen, Denmark.
6. Department of Plastic Surgery and Burns Treatment, Rigshospitalet, Copenhagen, Denmark.

These authors contributed equally to this work.

✉ Corresponding author: Professor Andreas Kjaer, MD, PhD, DMSc, Department of Clinical Physiology, Nuclear Medicine & PET, Rigshospitalet, National University Hospital - 4012, Blegdamsvej 9, 2100 - Copenhagen Ø, Denmark. E-mail: akjaer@sund.ku.dk

© 2015 Ivyspring International Publisher. Reproduction is permitted for personal, noncommercial use, provided that the article is in whole, unmodified, and properly cited. See <http://ivyspring.com/terms> for terms and conditions.

Received: 2015.06.15; Accepted: 2015.07.10; Published: 2015.09.13

Abstract

A first-in-human clinical trial with Positron Emission Tomography (PET) imaging of the urokinase-type plasminogen activator receptor (uPAR) in patients with breast, prostate and bladder cancer, is described. uPAR is expressed in many types of human cancers and the expression is predictive of invasion, metastasis and indicates poor prognosis. uPAR PET imaging therefore holds promise to be a new and innovative method for improved cancer diagnosis, staging and individual risk stratification. The uPAR specific peptide AE105 was conjugated to the macrocyclic chelator DOTA and labeled with ⁶⁴Cu for targeted molecular imaging with PET. The safety, pharmacokinetic, biodistribution profile and radiation dosimetry after a single intravenous dose of ⁶⁴Cu-DOTA-AE105 were assessed by serial PET and computed tomography (CT) in 4 prostate, 3 breast and 3 bladder cancer patients. Safety assessment with laboratory blood screening tests was performed before and after PET ligand injection. In a subgroup of the patients, the *in vivo* stability of our targeted PET ligand was determined in collected blood and urine. No adverse or clinically detectable side effects in any of the 10 patients were found. The ligand exhibited good *in vivo* stability and fast clearance from plasma and tissue compartments by renal excretion. In addition, high uptake in both primary tumor lesions and lymph node metastases was seen and paralleled high uPAR expression in excised tumor tissue. Overall, this first-in-human study therefore provides promising evidence for safe use of ⁶⁴Cu-DOTA-AE105 for uPAR PET imaging in cancer patients.

Key words: clinical trial, PET, uPAR

Introduction

Functional imaging with positron emission tomography (PET) allows for non-invasive characterization of tumor physiology with sensitivity in the pico-molar range. For this reason, PET imaging has been one of the fastest growing medical technologies during the last two decades. The majority of clinical PET imaging procedures worldwide are currently

performed with the glucose analogue ¹⁸F-fluorodeoxy-glucose (FDG) (1). FDG is taken up via specific glucose transporters (GLUT) in cancer cells. Unlike glucose, FDG is only a substrate for the initial hexokinase enzyme in the glycolysis and the monophosphate form of FDG is therefore trapped inside the cell. Through up-regulation of the insulin-independent

GLUT-1, enhanced FDG uptake and retention is observed for most cancer cells. However, there are inherent limitations in cancer imaging with FDG-PET due to multiple other non-cancerous causes of enhanced tissue glucose metabolism. Moreover, several FDG-PET studies have shown very limited or highly variable uptake in some cancer types most notably for prostate and breast cancer (2, 3). In other cancers, the method is limited by high uptake in surrounding tissue with glioblastoma as the most obvious example.

Due to these inherent limitations of FDG-PET and based on the increasing insight into tumor biology, many new targeting PET ligands have been identified and tested pre-clinically in various human xenograft cancer models. In line with this, at least one PET imaging ligand for each of the original hallmarks of cancer have been described. A number of these targeted PET ligands offer the potential to provide unique insight into cancer biology in real time in the natural microenvironment (4). However, despite an ever-increasing array of new PET ligands developed, primarily being tested in animal studies using dedicated small-animal PET systems, advancement of new PET ligands into human patients has been limited. The promise of new PET imaging ligands for cancer lies in the development and clinical validation of a stable ligand that is safe and with an optimal biodistribution pattern, including a specific binding mechanism based on cancer specific properties. Finally, a new PET imaging ligand should fulfill a clear clinical (unmet) need to succeed.

We developed a highly specific peptide-based PET imaging ligand, targeting the urokinase-type plasminogen activator receptor (uPAR). Extensive amount of studies have implicated the serine-protease urokinase-type plasminogen activator (uPA) and its receptor (uPAR) to be of special importance in cancer invasion and metastasis (5-9). In line with this, several studies have reported uPAR to have significant prognostic information in various cancers such as breast (10, 11), lung (12, 13), colorectal (9, 14), prostate (15-17) and bladder cancer (18). In these studies elevated expression levels of uPAR in the tumor or soluble fragments of uPAR in plasma have been shown to be strongly associated with metastatic disease, i.e. cancer aggressiveness, and subsequent poor prognosis. Thorough studies by immunohistochemistry and *in situ* hybridization have revealed low expression levels of uPAR in normal homeostatic tissues compared with malignant cancer lesions. Collectively this highlights uPAR as a potential ideal target for both imaging and therapy of 'invasion & metastasis', one of the originally described hallmarks of cancer (5, 19-21). ^{64}Cu -DOTA-AE105 is a novel clinical PET ligand for imaging of uPAR that is based on the high affinity

peptide antagonist AE105 (22). Extensive pre-clinical PET imaging validation studies have been reported in recent years with this PET ligand including a proof-of-concept study (23), a target validation study with demonstration of a differentiated tumor uptake compared to FDG (24), a comparative study with other ^{64}Cu -based uPAR PET ligands (25) and finally a human dosimetry estimate study in mice (26). Based on these promising preclinical results, combined with the strong biomarker potential of uPAR in human cancer, we hypothesize that ^{64}Cu -DOTA-AE105 could become a successful clinical uPAR PET imaging ligand. Such a PET ligand could become a *game-changer* in the management of cancer patients.

As the first step towards clinical translation of this ^{64}Cu labeled DOTA-conjugated peptide ligand for PET imaging of uPAR, we now report data from the first-in-human clinical trial of ^{64}Cu -DOTA-AE105, which received approval from the Danish Health and Medicines Authority (EudraCT no: 2013-002234-20). The protocol for this first-in-human trial included toxicological evaluation following the outlined principles described in the EMA adopted ICH guideline M3 (R2) *on non-clinical studies for the conduct of human clinical trials and marketing authorization for pharmaceuticals*, using the microdose approach (27).

The phase I clinical trial was conducted to evaluate the safety, pharmacokinetic and dosimetry of a single-dose injection in cancer patients using PET/CT imaging (Fig. 1). Safety measures included monitoring of blood pressure before, during and after the last imaging session, radiation exposure calculation (dosimetry) and plasma biochemistry before and after the study. Stability from plasma and urine analyses were also performed. Secondary objectives were to investigate the uptake in primary tumor lesions and potential metastases. Our data demonstrates that systemic administration of ^{64}Cu -DOTA-AE105 is safe with a favorable biodistribution and exhibits satisfactory *in vivo* stability. Specific tumor uptake in both primary lesions and metastatic lymph nodes of three cancer types were studied with promising results. We firmly believe that our data supports to proceed with a large-scale clinical trial focused on targeting an important receptor of the metastasis/invasiveness hallmark of cancer.

Results

Clinical trial design

Between May and August 2014, a total of 10 patients were PET/CT scanned with ^{64}Cu -DOTA-AE105 (EudraCT no: 2013-002234-20, ClinicalTrials.gov ID NCT02139371), 4 patients with prostate cancer, 3 patients with breast cancer and 3 patients with dissem-

inated bladder cancer (Fig. 1, B and C). The administered dose activity was 204 ± 6 MBq (range: 197-213 MBq) with a purity > 95% (table S1 and fig. S1) and the corresponding total peptide was 1.27 ± 0.27 μ g (range: 0.98-1.74 μ g) mass per patient. One patient did not complete all three PET/CT scans due to claustrophobia and was withdrawn from the study after completing the first 1 hour scan (patient 9).

PET ligand biodistribution and pharmacokinetics

The biodistribution profile of ^{64}Cu -DOTA-AE105 was investigated with whole-body PET/CT scans 1, 3 and 24 hours post injection (Fig. 2, A and B, fig. S2). Activity washout from most organs and lesions was observed in images of the late scan (24 hours), whereas activity retention in the liver and activity accumulation in the intestines became increasingly apparent. No activity was visible in the renal collecting system or urinary bladder at the late time point. Highest peak of activity was found in the bladder followed by liver, kidney and pancreas, respectively.

No activity was found in the brain. Three out of 10 patients in the study were used for investigating the plasma pharmacokinetics of ^{64}Cu -DOTA-AE105. Quantitative analysis of plasma samples with reversed phase high performance liquid chromatography (RP-HPLC) chromatogram revealed a plasma half-life of 8.5 min. (Fig. 3A). A representative radio (RP-HPLC) chromatogram profile from one patient (pt. 10) is shown in Fig. 3B, where intact ^{64}Cu -DOTA-AE105 could be found in plasma for up to 30 min post injection ($R_t=11.8$ min). One major metabolite was formed with a slightly more hydrophilic nature ($R_t=11.1$ min). Within the first hour post injection >40 MBq was found in the collected urine (Fig. 3C). Radio RP-HPLC analysis of collected urine revealed similar results as for plasma kinetics. 50 min post injection, a single metabolite could be found with similar retention time ($R_t=11.1$ min) as observed in plasma (Fig. 3D). No intact ^{64}Cu -DOTA-AE105 was found in the urine.

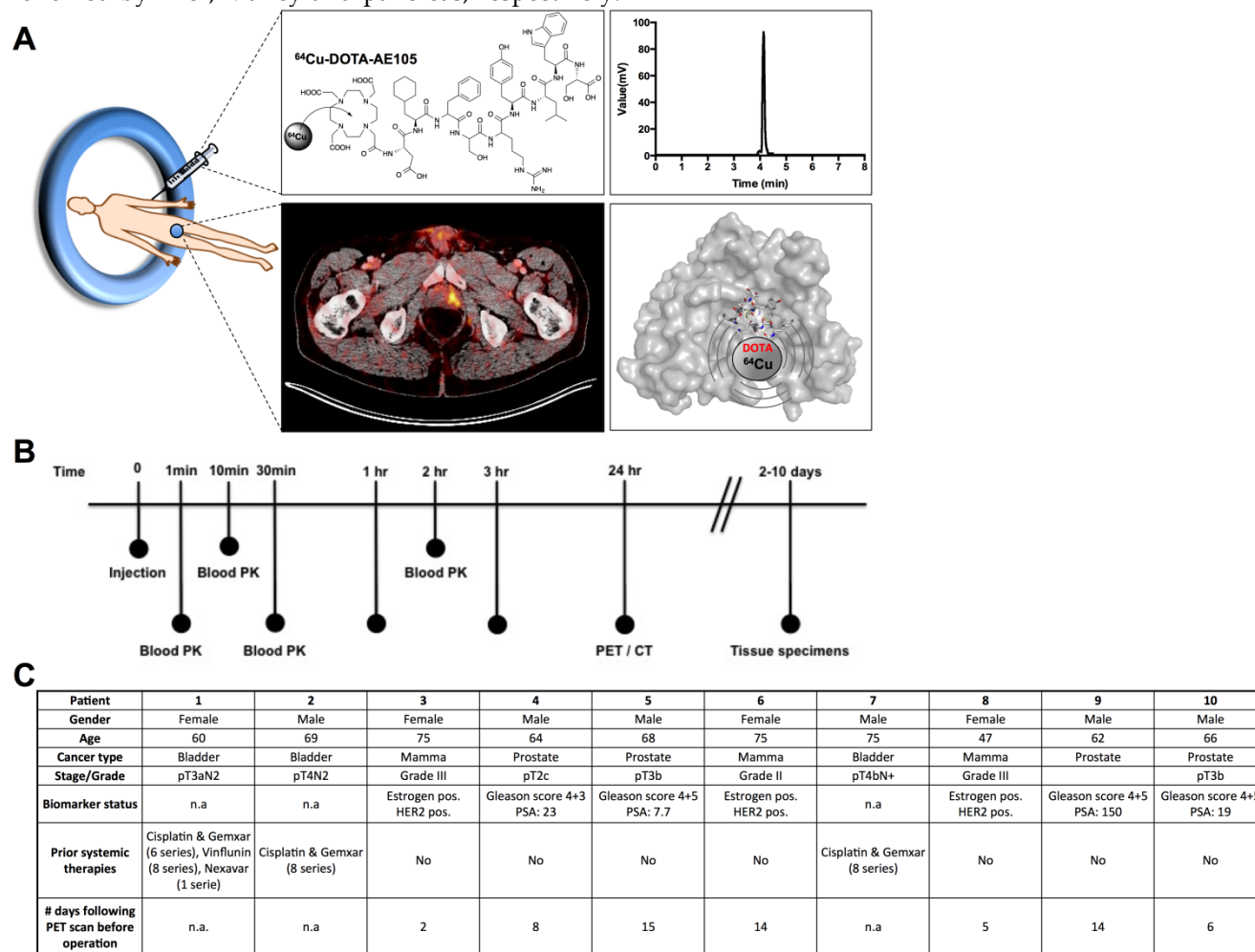


Fig. 1. uPAR PET imaging and overview of first-in-human uPAR PET study design. (A) Schematic of the uPAR PET ligand ^{64}Cu -DOTA-AE105 showing the chemical structure, a chromatogram of the final product, a transverse PET/CT image from a prostate cancer patient with tumor uptake of ^{64}Cu -DOTA-AE105 and a Pymol visualization of uPAR (surface representation) in complex with the targeting peptide shown as a cartoon representation. (B) Clinical trial events after single dose injection of ^{64}Cu -DOTA-AE105. Timeline denotes injection, acquisition of serial PET/CT imaging, and collection of blood and tissue specimens. (C) Patient characteristics.

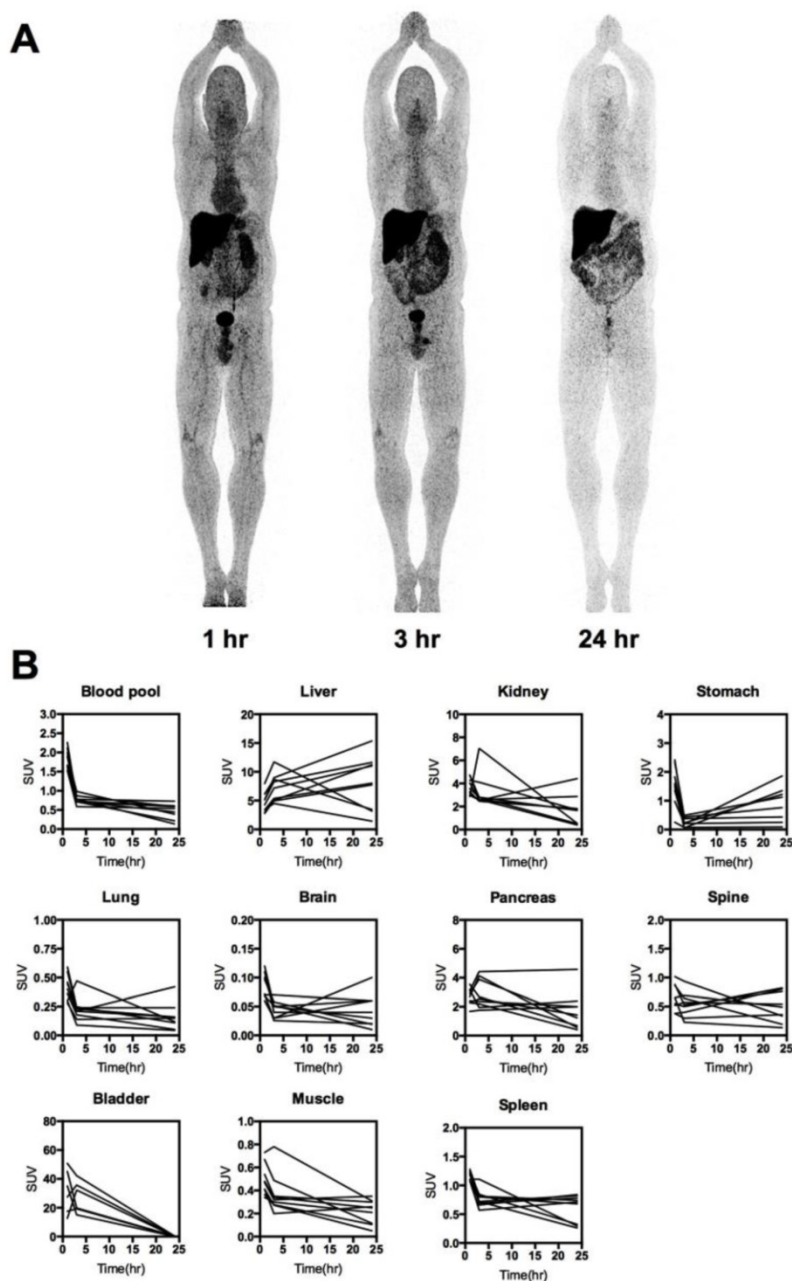


Fig. 2. Whole-body distribution and PK of ^{64}Cu -DOTA-AE105. (A) Maximum intensity projection PET images at 1, 3 and 24 hours following injection of ^{64}Cu -DOTA-AE105 (patient 10). The highest accumulation of activity was in the liver, bowel and bladder. **(B)** Decay corrected SUV values in blood and major organs plotted individually for $n = 10$ patients. For each patient ROIs were drawn on selected organ/tissue of interest at all three consecutive PET scans.

Patient safety and dosimetry

No infusion-related reactions or adverse events were noticed in any of the 10 patients following administration of ^{64}Cu -DOTA-AE105 in this study. There were no clinically detectable pharmacologically effects of ^{64}Cu -DOTA-AE105 and no apparent changes in general well being or vital signs. No long-term effects on blood parameters and/or organ functions were found when investigating standard biochemical parameters before and after enrollment in this study (fig. S3, table S2 and table S3). One patient (pt. 1) was hospitalized at the day of the last PET/CT scan due to

urinary tract infection and responded promptly to antibiotic treatment. Absorbed dose estimates based on a measured urinary excretion fraction of 37%, with a presumed 1-h voiding interval and a biologic half-life of 1.14 h are shown in Fig. 4A. A representative whole-body PET/CT 1, 3 and 24 hours post injection is shown in Fig. 4B. For dosimetry calculations, biodistribution data from 6 patients were used (table S4 and table S5). The three patients with bladder cancer were not included in the analysis due to a likely confounding effect on the glomerular filtration rate by the disease confined to the urinary system.

Patient 9 was also excluded due to missing data at 3 and 24 hours. The dose calculations yielded an effective dose of 0.0276 mSv/MBq. The liver was the organ with the highest absorbed dose (0.175 mGy/MBq), followed by the kidney (0.0562 mGy/MBq).

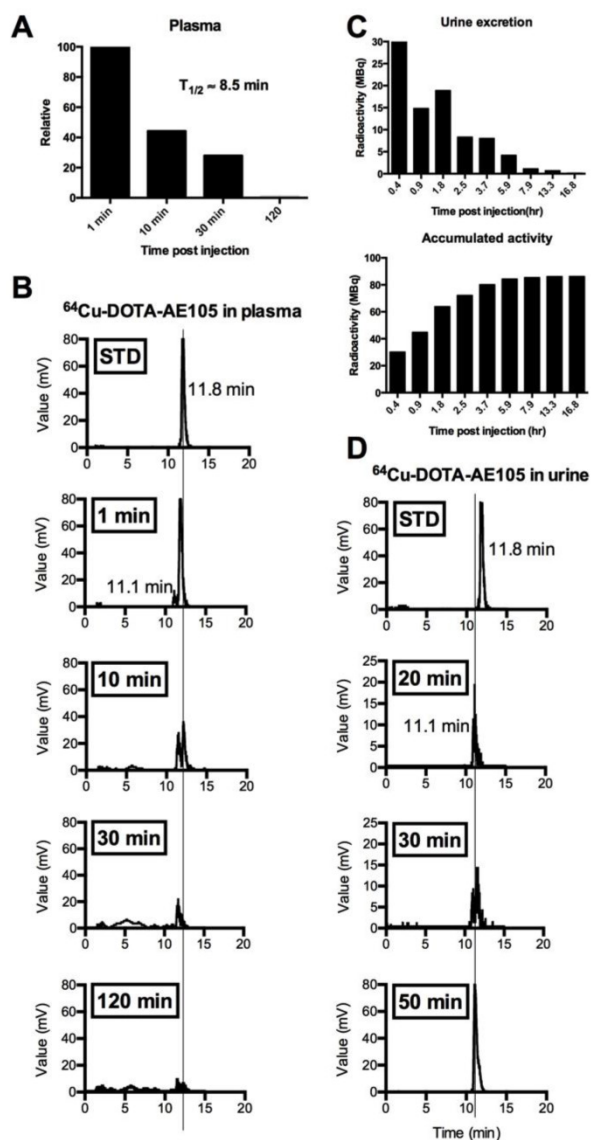


Fig. 3. Metabolic analysis of ^{64}Cu -DOTA-AE105 in plasma and urine. Data are shown for patient 10. **(A)** Relative time-dependent activity concentrations in plasma. Plasma half life was estimated to 8.5 min. **(B)** Chromatograms of ^{64}Cu -DOTA-AE105 in plasma. Data are shown for standard ($R_t=11.8$ min) and for the time points: 1, 10, 30 and 120 minutes. A single metabolite was formed ($R_t=11.1$ min) Vertical lines discriminate peaks corresponding to the uPAR PET ligand ^{64}Cu -DOTA-AE105. **(C)** Urine collection data. Time-dependent excretion of activity (top) and accumulated activity (bottom) are displayed. **(D)** Chromatograms of ^{64}Cu -DOTA-AE105 in urine. Data are shown for standard ($R_t=11.8$ min) and for the time points 20, 30 and 50 minutes. A single metabolite was found ($R_t=11.1$ min), corresponding to the single metabolite formed in plasma.

PET imaging with ^{64}Cu -DOTA-AE05: clinical case studies

PET/CT imaging with ^{64}Cu -DOTA-AE105 performed well in all three patients with bladder cancer

(patient 1, 2 and 7) (Fig. 5, A and B, Table 1) and identified both primary tumor (patient number 7) and metastatic lesions (all patients). We found a favorable biodistribution and high tumor-to-background uptake, especially in patient number 7 who was newly diagnosed with bladder cancer and untreated at the time of the ^{64}Cu -DOTA-AE105 PET/CT. In an organ based visual comparison of ^{64}Cu -DOTA-AE105 PET and CT, all lesions were detected on both modalities, except for three liver metastases in patient 2, that was not delineated at ^{64}Cu -DOTA-AE105 PET but only detected on contrast enhanced diagnostic CT at 1 hour (Table 1).

In breast cancer patients (patient 3, 6 and 8), the primary tumor was clearly visualized with high contrast on the ^{64}Cu -DOTA-AE105 PET/CT at all three time points (Fig. 6, A and B, Table 1). Washout of radioactivity was slower in tumors than in normal organs, resulting in steadily increasing tumor-to-organ ratios over time except for the tumor-to-liver ratio that decreased over time and at all three time points remained below 1. Patient 8 was subsequently diagnosed with lymph node involvement, and in this patient the two malignant axillary lymph nodes were visually detected on the ^{64}Cu -DOTA-AE105 PET (Fig. 6B). Immunohistochemical (IHC) staining of uPAR on surgical resected primary breast tumor tissue confirmed uPAR positive cancer cells in all three patients (fig. S4A). In patient 6, a slightly uPAR-positive lesion was encountered in the meninges of the brain with typical features of a previously not diagnosed meningioma on CT and on a subsequent MRI (fig. S5).

Finally, in the four patients with newly diagnosed and biopsy-proven prostate cancer (patient 4,5,9 and 10) a high and specific uptake in primary cancer tumor lesions was found (Fig. 7, A and B, Table 1). One patient (patient 9) had several visible uPAR PET positive lymph nodes in the pelvic region. This was confirmed during the operation where the surgeon found several enlarged lymph nodes suspected to be malignant. The patient was accordingly not prostatectomized and six lymph nodes were removed with histopathological confirmation of prostate adenocarcinoma in 3 lymph nodes. Two patients had no signs of metastases on neither uPAR-PET nor perioperative staging. However in patient five 17 regional lymph nodes were removed and prostate adenocarcinoma was found in one lymph node. This lymph node metastasis was not visualized on the uPAR-PET or CT. However, uPAR IHC on removed prostate cancer tissue in all three patients, confirmed general pattern of uPAR expression (fig. S4B).

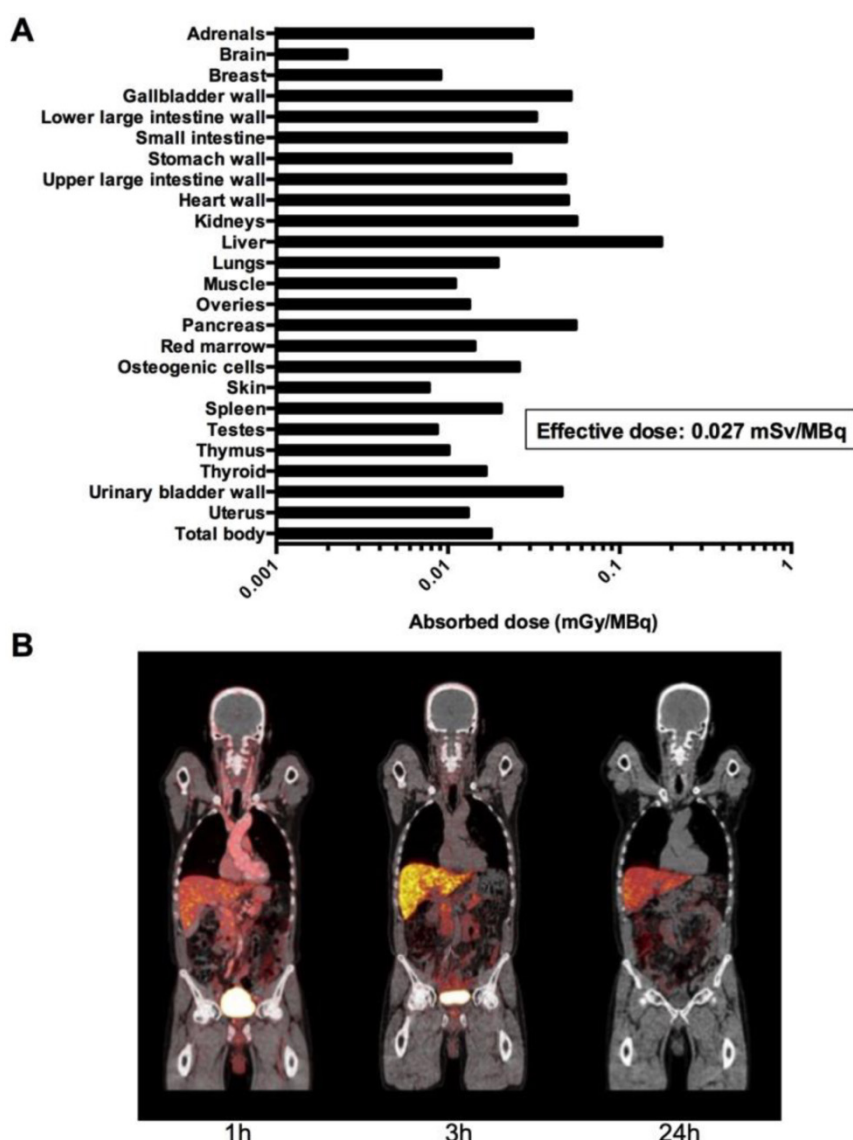


Fig. 4. Dosimetry and whole-body PET/CT imaging of ⁶⁴Cu-DOTA-AE105. (A) Mean absorbed dose per unit administered (mGy/MBq) of major organs and tissues (table S4) were derived from 6 patients (patient 3,4,5,6,8 and 10) from serial whole-body PET scans acquired over 24 hours time interval following injection of ⁶⁴Cu-DOTA-AE105 using VOI-based time activity data (table S5). **(B).** Coronal whole-body PET/CT images (patient 5) show time dependent biodistribution at 1,3 and 24 hours and demonstrates accumulation of activity mainly in the liver and bowel.

Table I: Summary of uPAR PET/CT results clinical workup

Patient #	uPAR PET	Routine clinical CT	Operation	uPAR PET vs. Clinical CT or operation	Mean	Max
Primary tumor detection					SUV 1 hour	
1	Primary tumor surgically removed	Primary tumor surgically removed	Previously performed	na	na	na
2	Primary tumor surgically removed	Primary tumor surgically removed	Previously performed	na	na	na
3	1 Breast lesion	Not performed	Breast cancer confirmed	1 out of 1	1.5	3.8
4	1 Prostate lesion	Not performed	Prostate cancer confirmed	1 out of 1	2.8	9.3
5	1 Prostate lesion	Not performed	Prostate cancer confirmed	1 out of 1	2.1	7.7
6	1 Breast lesion	Not performed	Breast cancer confirmed	1 out of 1	1.3	2.9
7	1 bladder lesion	1 bladder lesion	No operation	1 out of 1	2.3	15.9
8	1 Breast lesion	Not performed	Breast cancer confirmed	1 out of 1	1.1	4.0
9	1 Prostate lesion	Not performed	Prostate cancer confirmed from biopsy	1 out of 1*	2.9	12.5
10	1 Prostate lesion	Not performed	Prostate cancer confirmed	1 out of 1	2.8	8.9
Metastasis detection					SUV 1 hour[^]	
1	2 inguinal lymph node and 1 abdominal metastases	2 inguinal lymph node and 1 abdominal metastases	Previously performed	3 out of 3	1.5	4.6

Patient #	uPAR PET	Routine clinical CT	Operation	uPAR PET vs. Clinical CT or operation	Mean	Max
2	1 retroperitoneal lymph node	1 retroperitoneal lymph node and 2 liver metastases	Previously performed	1 out of 3	1.5	3.5
3	No metastases	Not performed	No metastases	0 out of 0	-	-
4	No metastases	No metastases	No metastases	0 out of 0	-	-
5	No metastases	Not performed	1 metastasis	0 out of 1	-	-
6	No metastases §	Not performed	No metastases	0 out of 0	-	-
7	>6 abdominal/pelvic lymph node metastases	>6 abdominal/pelvic lymph node metastases	No operation	>6 our of >6	4.3	7.8
8	2 axillary lymph node metastases	Not performed	2 axillary lymph node metastases	2 out of 2	0.9	3.2
9	8 visible lymph nodes, 1 lymph node > 10 mm	Several visible lymph nodes 1 lymph node >10 mm	No operation	na*	-	-
10	No metastases	No metastases	No metastases	0 out of 0	-	-

* No prostatectomy was performed. Prostate adenocarcinoma in 6 of 6 preoperative biopsies. During the open operation several lymph nodes were judged visually to be malignant. Six lymph nodes were removed, 3 of these with prostate adenocarcinoma.

§ 1 uPAR PET positive lesion in brain/meninges (subsequent MRI of the brain showed typically meningioma (Fig. S5))

^The value displayed is the metastasis with highest uptake if multiple metastases were present.

- Not relevant.

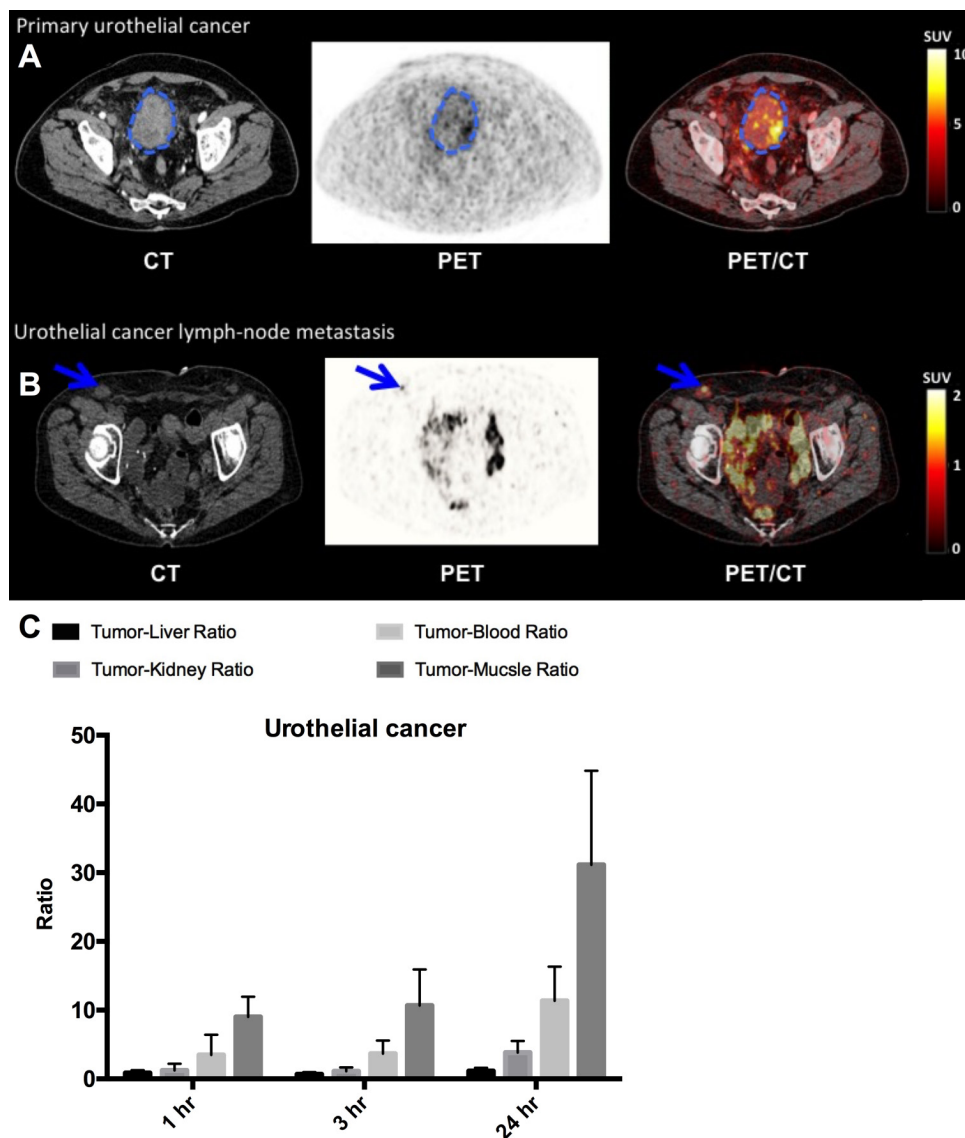


Fig. 5. uPAR PET imaging in bladder cancer. (A) Representative transverse CT, PET and co-registered PET/CT images of a primary tumor lesion (blue circle), top images, with intense uptake of ⁶⁴Cu-DOTA-AE105 (patient 7). (B) Bottom images show a uPAR positive inguinal lymph node metastasis (blue arrow) with high uptake (patient 1). (C) Tumor-to-liver, tumor-to-blood, tumor-to-kidney and tumor-to-muscle ratios as a function of time post injection. Data are averages ± SD (n = 1 ROI per time point, n = 3 patients).

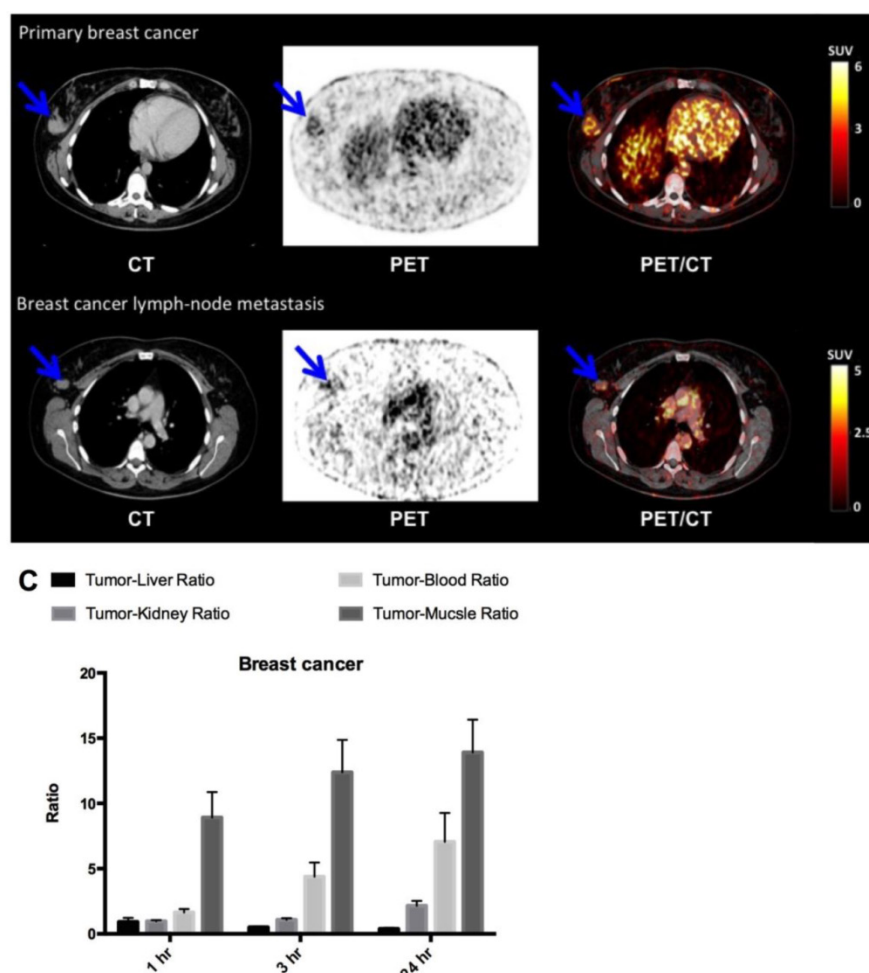


Fig. 6. uPAR PET imaging in breast cancer. (A) Representative transverse CT, PET and co-registered PET/CT images of a primary tumor lesion (blue arrow), top images, with intense uptake of ^{64}Cu -DOTA-AE105 (patient 8). (B) Bottom images show an uPAR positive axillary lymph node metastasis (blue arrow) with high uptake in the same patient. (C) Tumor-to-liver, tumor-to-blood, tumor-to-kidney and tumor-to-muscle ratios as a function of time post injection. Data are averages \pm SD ($n = 1$ ROI per time point, $n = 3$ patients).

Discussion

Our first-in-human study of a uPAR PET ligand is the culmination of more than 6 years of translational uPAR PET research of our group and build on more than 30 years of basic research in the uPAR performed at Rigshospitalet in Copenhagen (28). Importantly, in our study all examined primary tumors were positive on uPAR PET and the majority of metastases were identified (Table 1). The study thus provides the first evidence of uPAR as a promising imaging target across three human cancer types for both primary and metastatic lesions detection.

With the demonstration of uPAR expression in nearly all cancer types and establishment of uPAR as a strong prognostic factor, uPAR must also be considered a promising imaging target (29). Successful development and clinical validation of uPAR PET imaging could potentially fulfill several clinical applications, including *I*) identification of the aggressive cancer phenotype, *II*) staging of uPAR positive can-

cers, and *III*) identification of patient eligible for uPAR targeted therapies and subsequent treatment monitoring. Of particular interest, uPAR has been shown to be highly expressed and to be a strong prognostic factor in several cancer types where FDG-PET imaging is not routinely used, including prostate, breast and bladder cancer (10, 15, 18).

In prostate cancer, we found that 4 out of 4 primary tumors were positive and several lymph node metastases were identified (Fig. 7, Table 1). In contrast, a recent first-in-human phase I PET study using a bombesin analogue in 10 prostate cancer patients reported only uptake in 5 out of 10 primary lesions (30) indicating a superior performance of uPAR PET compared to PET imaging of the gastrin-releasing peptide receptor in prostate cancer. We found a favorable tumor-to-background ratio in both primary tumor lesions and metastatic lymph nodes in breast and bladder cancer patients, collectively providing strong evidence for the potential for uPAR PET/CT in breast, bladder and prostate cancer patients. In addi-

tion, target specific uptake of the ^{64}Cu -DOTA-AE105 in both breast and prostate tumor lesions was supported by *ex vivo* immunohistochemistry that clearly demonstrated uPAR expression in excised tissue in all patients. Interestingly, soluble uPAR forms in plasma were only elevated in two out of ten patients, when compared to healthy individuals (fig. S6), despite confirmed cancer disease in all ten patients. This underlines the different kind of information uPAR PET imaging provides, compared to uPAR plasma assays.

The overall aim of this *first-in-human* clinical trial was to investigate the safety and dosimetry properties of ^{64}Cu -DOTA-AE105. ^{64}Cu -DOTA-AE105 was well tolerated and there were no adverse events or obvious changes in general well-being or any vitals signs (fig. S3, table S2 and table S3). An effective radiation dose of 0.0276 mSv/MBq was found, equaling 5.5 mSv at an injected activity of approximately 200 MBq as used by us. This is similar to the radiation dose received from a standard FDG-PET, where the effective dose is approximately 0.019 mSv/MBq, equal to 5.7 mSv at a

dose of 300 MBq (31, 32). Therefore, the radiation burden of uPAR PET with ^{64}Cu -DOTA-AE105 is of no major clinical concern and the effective dose of ^{64}Cu -DOTA-AE105 is comparable to that of other clinically applied ^{64}Cu -based PET ligands (33-37). Whether this dosimetry estimation also reflects potential future uPAR PET imaging ligands based on AE105 with different isotopes such as Ga-68 and F-18 needs to be shown when the biodistribution profile for these variants are known. Interestingly, our previous report on human dosimetry estimate of ^{64}Cu -DOTA-AE105 projected from mouse biodistribution data (26), only deviated less than 10% from the true observed value in the present study (0.0251 mSv/MBq vs. 0.0276 mSv/MBq). Similar agreement was also found in another *first-in-human* study performed by us, namely ^{64}Cu -DOTA-TATE (35). Accordingly, human effective dose estimates obtained from mouse studies seem accurate, at least for Cu-labelled peptide based PET ligands.

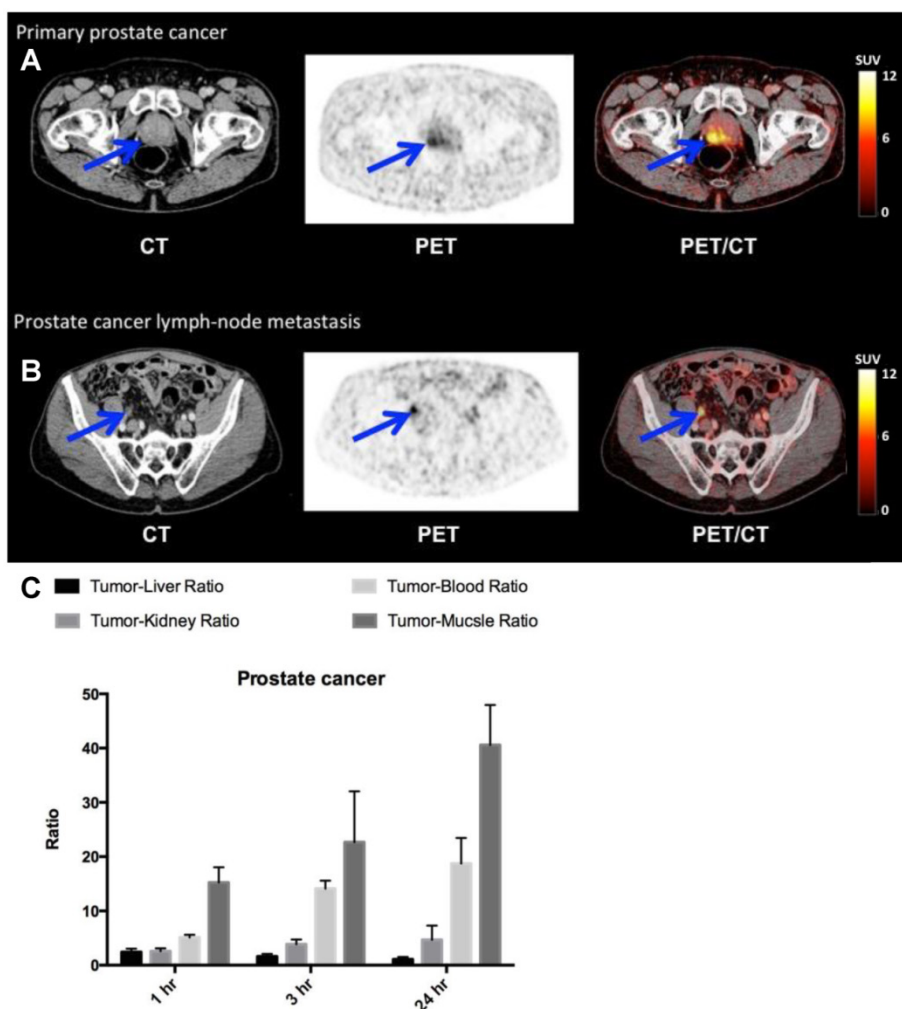


Fig. 7. uPAR PET imaging in prostate cancer. (A) Representative transverse CT, PET and co-registered PET/CT images of a primary tumor lesion (blue arrow), top images, with high uptake of ^{64}Cu -DOTA-AE105 (patient 4). (B) Bottom images show an uPAR positive regional lymph node metastasis (blue arrow) with high uptake (patient 9). (C) Tumor-to-liver, tumor-to-blood, tumor-to-kidney and tumor-to-muscle ratios as a function of time post injection. Data are averages \pm SD ($n = 1$ ROI per time point, $n = 3$ patients).

As expected, the biodistribution analysis revealed the liver to have a high accumulation of activity following injection of ^{64}Cu -DOTA-AE105 (Fig. 2, fig. S2, table S5), which most likely is caused by the known *in vivo* instability of the ^{64}Cu -DOTA complex (38, 39) and not specifically mediated by uPAR. This known *in vivo* instability of the ^{64}Cu -DOTA complex has prompted an extensive search for improved radionuclide metal chelators with higher stability for ^{64}Cu (40-42). Improved *in vivo* stability data have especially been reported for tetra-amine based macrobicyclic chelators, in which an ethylene bridge connects two nonadjacent nitrogens, compared to the monocyclic DOTA and TETA (43, 44). In particular, the use of CB-TE2A as chelator for ^{64}Cu has been used with success in a number of *in vivo* studies in animals (40, 45-47), including PET imaging of uPAR expression (25). Recently, the *first-in-human* bombesin PET study with ^{64}Cu -CB-TE2A-AR06 (37) was reported, where a significantly lower liver uptake was found compared to our study. This therefore seems to confirm the superior *in vivo* stability of CB-TE2A for chelating ^{64}Cu *in vivo* in humans. However, in a previous *first-in-human* study by our group using ^{64}Cu -DOTATATE (35) did not find the high non-specific liver uptake to limit the clinical usefulness of PET images as all liver metastases could still clearly be identified. In the present study, two metastatic lesions in the liver were not identified on uPAR PET/CT images, possible due to the high background uptake. However, scans at 1 h post injection seems to provided excellent contrast for both primary tumor lesions and lymph node metastases, making the use of ^{18}F or ^{68}Ga radionuclides promising for future clinical studies, thereby rendering the non-specific liver uptake of less importance.

Besides a relatively high non-specific uptake in the liver, no other organ/tissue showed high non-specific uptake of ^{64}Cu -DOTA-AE105. The blood pool clearance of ^{64}Cu -DOTA-AE105 was evident between the 1 hour and the 3 hour scan (Fig. 2, fig. S2, table S5), where the SUV was less than 1 g/mL. Plasma pharmacokinetic and urine metabolite analysis revealed a relatively fast formation of one metabolite in plasma with increased hydrophilic properties, which was subsequently also found in the urine of the patients (Fig. 3). No intact ^{64}Cu -DOTA-AE105 was found in the urine.

Besides being involved in the proteolytic process during cancer invasion and metastasis, the uPA/uPAR system plays an important part in modulating inflammatory processes, such as infection and chronic systemic inflammatory diseases e.g. rheumatoid arthritis or osteoarthritis (48, 49). Consistent with this, analysis of synovial tissue from rheumatoid ar-

thritis and osteoarthritis patients, and normal synovial tissue have revealed higher uPA activity and markedly increased expression of uPAR in the rheumatoid arthritis synovial tissue, especially at the marginal zone between pannus and cartilage. It is possible that uPAR PET imaging could also be useful for diagnosis and especially disease/treatment monitoring in such pathological conditions as well. In addition, recent studies have found uPAR to be associated with unstable, ruptured carotid plaques, making uPAR PET highly interesting for imaging of vulnerability and rupture of plaques (50, 51).

Currently, more than 90% of clinical PET studies are performed with the glucose analogue FDG(1). However, due to lack of sensitivity FDG-PET/CT is not part of the recommended diagnostic work-up in prostate, bladder, nor primary breast cancer with or without axillary nodal involvement. However, for initial and recurrent breast cancer staging, FDG-PET/CT has in many studies been demonstrated as more accurate than conventional imaging methods in detecting extra-axillary nodal involvement and distant metastases (52, 53). With the distinct high tumor uptake of ^{64}Cu -DOTA-AE105 in all three cancer types found by us, it seems possible that ^{64}Cu -DOTA-AE105 uPAR PET could become a promising method for staging, restaging and detection of relapse in these cancer forms. Moreover, ^{64}Cu -DOTA-AE105 uPAR PET possess the ability to generate prognostic information of value in treatment planning. Especially considering prostate cancer, a huge unmet clinical need exists for accurate risk stratification at time of diagnosis in order to reduce the significant overtreatment, e.g. unnecessary prostatectomies, currently being practiced (54). uPAR PET imaging seems to be a highly promising technology for this purpose, with strong prognostic information of uPAR in prostate cancer and the high and specific uptake found in the present study. However, large controlled clinical trials are necessary to prove this hypothesis.

Materials and Methods

Production of ^{64}Cu -DOTA-AE105

^{64}Cu was produced via the $^{64}\text{Ni}(p,n)^{64}\text{Cu}$ reaction using a solid target system comprising a water-cooled target mounted on the beam line of a PETtrace (GE Healthcare) cyclotron. DOTA-AE105 was labeled with ^{64}Cu by adding a solution of DOTA-AE105 (10 nmol) in aqueous ammonium acetate (1 mL; 0.1 M, pH 8.4 containing gentisic acid, 5 mg/mL) to a dry vial containing $^{64}\text{CuCl}_2$ (2000 MBq) in 500 μL sterile Traceselect water. The mixture was left at 80°C for 5 min and then diluted with sterile water (1 mL). The product

was purified with a SepPak light column and 9 mL saline was added. Finally, the mixture was passed through a Millex-GP 0.22-mm sterile filter (Millipore) (See process validation Table S6) and analytic validation (fig. S7) and release criteria (table S7). Radiochemical purity was determined by reversed-phase high-pressure liquid chromatography (RP-HPLC) (fig. S1). All chemicals were purchased from Sigma-Aldrich Denmark A/S unless specified otherwise. DOTA-AE105 was purchased from ABX GmbH (Advanced Biochemical Compounds, Radeberg, Germany). HPLC analysis was performed on a Dionex UltiMate 3000 HPLC with a Scansys radiodetector. ^{64}Cu -DOTA-AE105 was analysed on a Phenomenex Kinetex column (2.6 μm C18, 50 x 4.6 mm) with flow of 1.5 ml/min. The HPLC mobile phase was solvent A, 0.1 % TFA in MeCN:H₂O 10:90, and solvent B, 0.1 % TFA in MeCN:H₂O 90:10. Gradient: 0-1 min 10% B, 1-6 min 10-65% B, 6-7 min 65-10%B and 7-8 min 10% B. The retention time of ^{64}Cu -DOTA-AE105 was 4.1 min and the specific activity was determined by UV absorption at 228 nm

Study design

In total, 10 patients with histopathologically confirmed prostate cancer (4), breast cancer (3) or bladder cancer (3) were enrolled in the study from May 2014 to August 2014. Of these patients, six were used for dosimetry (3 prostate and 3 breast cancer patients). All patients had given written informed consent before inclusion. The study was approved by the Danish Health and Medicine Authority (EudraCT no: 2013-002234-20) and the Regional Scientific Ethical Committee (protocol H-2-2013-111). The study was registered in ClinicalTrials.gov under NCT02139371. The study was performed in accordance with the recommendation for Good Clinical Practice (GCP) and independently monitored by the GCP unit of the Capital Region of Denmark. The outline of procedures for each patient is shown in Fig. 1. In brief, the patient was injected intravenously with approximately 200 MBq of ^{64}Cu -DOTA-AE105 (table S1). This was followed by collection of blood after 1, 10 and 30 min post injection for pharmacokinetic analysis. Each patient was then whole-body PET/CT scanned 1, 3 and 24 hours post injection. Urine was furthermore collected from 3 patients during the entire 24 hour period. The patients with urinary bladder cancer were treated with chemotherapy during the time of the ^{64}Cu -DOTA-AE105 PET/CT (Fig. 1). Patients with breast and prostate cancer were not treated with chemotherapy at the time of the ^{64}Cu -DOTA-AE105 PET/CT and were subsequently treated with surgical removal of the primary tumor lesions, including sentinel node procedure (breast) and pelvic lymph node

dissection (prostate).

Plasma pharmacokinetics and urine metabolite analysis

The blood and urine samples were analyzed on a Dionex UltiMate 3000 column-switching HPLC system with a Posi-RAM Module 4. The blood samples (full blood) were centrifuged (3,500 rpm, 4 min) and the supernatant plasma was collected and filtered through a 0.45 μm syringe filter prior to the HPLC analysis(55). The HPLC analysis consisted of two steps, an extraction step and an analytical step, as previously described(56). During the extraction step, the plasma samples were passed through a shim-pack XR-ODS (30 x4.6 mm, 2.2 μm). The valves were switched and the sample was then analyzed on an Onyx monolithic column (C18, 50 x 4.6 mm). The mobile phase for the extraction step was 0.1 % TFA in H₂O, while the analytical step was a gradient method with solvent A, 0.1% TFA in MeCN: H₂O 10:90, and solvent B, 0.1% TFA in MeCN:H₂O 90:10, both with a flow of 1 ml/min. Gradient: 0-6 min (extraction), 6-7 min 0-10% B, 7-13 min 10-65% B, 13-14 min 65-10% B, 14-15 min 10% B.

PET/CT acquisition and image analysis

Data acquisition was performed using a Biograph mPET/CT scanner (Siemens Medical Solutions, Erlangen, Germany) with an axial field of view of 216 mm. After intravenous injection (i.v.) of 203.9 \pm 6.4 MBq of ^{64}Cu -DOTA-AE105, emission scans were acquired 1 h, 3 h, and 24 h post i.v. administration. Whole-body PET scans were obtained in 3-dimensional mode, with an acquisition time of 3 min per bed position. Attenuation and scatter corrected PET data were reconstructed iteratively using a 3D ordered-subset expectation-maximization algorithm including point spread function and time of flight information (Siemens Medical Solutions), the settings were, 2 iterations, 21 subsets, 2 mm Gaussian filter and a 400 x 400 matrix, Pixel size in the final reconstructed PET image was approximately 2 x 2 mm with a slice thickness of 2 mm. A diagnostic CT scan was obtained before the first PET scan, with a 2-mm slice thickness, 120 kV, and a quality reference of 225 mAs modulated by the Care Dose 4D automatic exposure control system (Siemens Medical Solutions). A low-dose CT scan, 2-mm slice thickness, 120 kV, and 40 mAs, was acquired before each of the subsequent scans and used for attenuation correction. An automatic injection system was used to administer 75 mL of an iodine containing contrast agent (Optiray 300; Covidien, Minneapolis, MN, USA) with a scan delay of 60 s and flow rate of 1.5 mL/s, followed by an injection of 100 mL of NaCl with a flow rate of 2.5

mL/s. Furthermore, patients had been asked to drink 500 mL of water 25 min before image acquisition. PET images in units of Bq/mL were used for quantitative analysis of tissue radioactivity concentrations for dosimetry purposes and for calculation of standardized uptake values (SUV). The latter uptake characteristic was obtained by drawing three representative spheric volumes of interest (VOIs) in the organ/tissue of interest. For the calculation of absorbed dose estimates, we assumed a uniform distribution of radioactivity concentrations throughout the source organs.

Dosimetry

Dosimetry was based on the decay-uncorrected image sets from the 3 time-points (6 patients) supplemented with the 24 hour sampled urine-data (3 patients). The 24 hours urine were collected in pre weight plastic bottles and for each individual voiding the weight (volume) were measured and a 500 μ L sample were drawn for activity measurement in a calibrated gamma well counter (Cobra II TM, Gamma Counting Systems; PACKARD, Meriden, CT, USA). For each patient, organ and time-point, activity concentration was calculated as the average of the values from 3 VOIs, and total activity estimated by multiplying these average values by organ masses of the OLINDA male adult phantom. As a surrogate for red marrow activity, VOIs were drawn encompassing large portions of the L3-L5 vertebrae. Cumulated activity for each patient and organ was determined by integration of time-activity curves, constructed as a linear piece from zero at injection to the first measuring point and mono-exponentials between the measuring points. Beyond 24 h (last imaging point), removal by simple physical decay was assumed. For each patient, cumulated organ values were normalized by division with injected activity and finally, for each organ, values were averaged over the 6 patients. Individual urine excretion data were fitted to mono-exponentials yielding the fraction of injected activity excreted and a biological half-life of the process. Values were averaged over the 3 patients. The value assigned to the remainder of the body was derived as the residual between the total cumulated activity (as calculated from the nuclide's half-life) minus all activity accounted for in specific organs (including muscle) or by excretion. All data were entered into OLINDA/EXM software (Vanderbilt University, Nashville, TN, USA) to obtain corresponding estimates of organ-absorbed doses and effective dose. OLINDA's Voiding Bladder Model was used with fraction and half-life from the fitted urine data as input and an assumed bladder voiding interval of 1 hour

Tumor uptake by visual image analysis and activity quantification

All image data were analysed by a team consisting of a highly experienced certified specialist in nuclear medicine and a highly experienced certified specialist in radiology. Tumor uptake analyses were limited to lesions identifiable on CT and uptake characteristics were obtained by drawing spheric volumes of interest (VOIs) sufficiently large to encompass the tumor lesion. Standardized uptake values were calculated from the generated VOIs for all three PET/CT scans (1, 3 and 24 hours post injection) and parameterized as SUV_{mean} and SUV_{max} .

Histology

The mean time interval between PET and surgery was 5 days. Resected tissue samples obtained from the ^{64}Cu -DOTA-AE105 imaged primary tumors were placed in formalin. Sections were prepared with paraffin sections (2.5 μ m thick) and a standard immunohistochemistry technique (avidin-biotin-peroxidase) was performed as described in a previous study (24), to visualize the immunostaining intensity and distribution of uPAR receptors. In addition, HE staining was performed. The sections were visually evaluated for visible uPAR positive staining.

uPAR forms in plasma

Soluble uPAR forms were measured in EDTA plasma samples in all 10 patients using time-resolved fluorescence immunoassays as recently described in details elsewhere (57). Mean levels in pmol/L with %CV values can be found in fig. S6 together with the reference levels in healthy individuals at the age of 60 (adapted from (57)).

Statistics

All statistical analyses were performed using GraphPad Prism version 6.0 for MAC OS X (GraphPad Software Inc., USA). All comparisons between the treatment groups were performed using two-side student t-test. $P < 0.05$ was considered statistically significant. All data are presented as mean \pm SD.

Supplementary Material

Figures S1-S7 and Tables S1-S7.

<http://www.thno.org/v05p1303s1.pdf>

Acknowledgments

This work was supported by the John and Birthe Meyer Foundation, the Danish National Advanced Technology Foundation, the Research Foundation of Rigshospitalet, the Capital Region of Denmark, the

Novo Nordisk Foundation, the Lundbeck Foundation, the A.P. Moeller Foundation, the Svend Andersen Foundation, the Arvid Nilsson Foundation and the Danish Council for independent research.

The authors would like to thank all patients and their families for participating in this study. In addition, we will thank the staff at the department of Clinical Physiology, Nuclear Medicine and PET, Rigshospitalet for participating in the conduction of the study.

Author contributions

MPE, DS and AK initiated and designed the study. MP designed the uPAR targeting peptide. MBL, CC and JM were responsible for production of ⁶⁴Cu-DOTA-AE105 and analysis of radioactive metabolites. HP, KB and NK recruited patients and provided clinical data. ALJ and AKB evaluated and scored PET/CT scans. TLK and SH performed dosimetry calculations. MP and TT were in charge of uPAR plasma analyses and IHC. MPE, DS, CHN, LH and AK analyzed and interpreted data. MPE, DS and AK drafted the manuscript with input from other authors. All authors reviewed and contributed in revisions of manuscript as well as approved the final version. AK takes overall responsible for the content of the manuscript.

Competing interests

MPE, JM & AK are inventor of a patent on the composition of matter of uPAR PET. MPE, JM, CHN & AK are co-founders of a start-up company (Curasight) that has licensed the uPAR PET patent and is currently raising funds to commercialize uPAR PET technology. Pending patent for MPE, JM & AK: *Positron Emitting Radionuclides Labeled Peptides for Human uPAR PET Imaging* (WO 2014/086364 A1). The authors declare that their spouses, partners, or children have no financial relationships relevant to the submitted work. Inquiries should be directed to the corresponding author.

References

- Gambhir SS. Molecular imaging of cancer with positron emission tomography. *Nat Rev Cancer*. 2002;2(9):683-93.
- Kayani I, and Groves AM. 18F-fluorodeoxyglucose PET/CT in cancer imaging. *Clinical medicine*. 2006;6(3):240-4.
- Rohren EM, Turkington TG, and Coleman RE. Clinical applications of PET in oncology. *Radiology*. 2004;231(2):305-32.
- Weber WA, Czernin J, Phelps ME, and Herschman HR. Technology Insight: novel imaging of molecular targets is an emerging area crucial to the development of targeted drugs. *Nature clinical practice Oncology*. 2008;5(1):44-54.
- Persson M KA. Urokinase-type plasminogen activator receptor (uPAR) as a promising new imaging target: potential clinical applications. *Clinical Physiology and Functional Imaging*. 2013.
- Jacobsen B, and Ploug M. The urokinase receptor and its structural homologue C4.4A in human cancer: expression, prognosis and pharmacological inhibition. *Curr Med Chem*. 2008;15(25):2559-73.
- Dass K, Ahmad A, Azmi AS, Sarkar SH, and Sarkar FH. Evolving role of uPA/uPAR system in human cancers. *Cancer Treat Rev*. 2008;34(2):122-36.

- Dano K, Behrendt N, Hoyer-Hansen G, Johnsen M, Lund LR, Ploug M, and Romer J. Plasminogen activation and cancer. *Thromb Haemost*. 2005;93(4):676-81.
- Ganesh S, Sier CF, Heerding MM, Griffioen G, Lamers CB, and Verspaget HW. Urokinase receptor and colorectal cancer survival. *Lancet*. 1994;344(8919):401-2.
- Foekens JA, Peters HA, Look MP, Portengen H, Schmitt M, Kramer MD, Brunner N, Janicke F, Meijer-van Gelder ME, Henzen-Logmans SC, et al. The urokinase system of plasminogen activation and prognosis in 2780 breast cancer patients. *Cancer Res*. 2000;60(3):636-43.
- Riisbro R, Christensen IJ, Piironen T, Greenall M, Larsen B, Stephens RW, Han C, Hoyer-Hansen G, Smith K, Brunner N, et al. Prognostic significance of soluble urokinase plasminogen activator receptor in serum and cytosol of tumor tissue from patients with primary breast cancer. *Clinical cancer research: an official journal of the American Association for Cancer Research*. 2002;8(5):1132-41.
- Pappot H, Hoyer-Hansen G, Ronne E, Hansen HH, Brunner N, Dano K, and Grondahl-Hansen J. Elevated plasma levels of urokinase plasminogen activator receptor in non-small cell lung cancer patients. *Eur J Cancer*. 1997;33(6):867-72.
- Pappot H, Pfeiffer P, Grondahl-Hansen J, and Skov B. Presence of urokinase plasminogen activator, its inhibitor and receptor in small cell lung cancer and non-small cell lung cancer. *Int J Oncol*. 1997;10(1):177-82.
- Pyke C, Ralkiaer E, Ronne E, Hoyer-Hansen G, Kirkeby L, and Dano K. Immunohistochemical detection of the receptor for urokinase plasminogen activator in human colon cancer. *Histopathology*. 1994;24(2):131-8.
- Almasi CE, Brasso K, Iversen P, Pappot H, Hoyer-Hansen G, Dano K, and Christensen IJ. Prognostic and predictive value of intact and cleaved forms of the urokinase plasminogen activator receptor in metastatic prostate cancer. *Prostate*. 2011;71(8):899-907.
- Shariat SF, Roehrborn CG, McConnell JD, Park S, Alam N, Wheeler TM, and Slawin KM. Association of the circulating levels of the urokinase system of plasminogen activation with the presence of prostate cancer and invasion, progression, and metastasis. *J Clin Oncol*. 2007;25(4):349-55.
- Miyake H, Hara I, Yamanaka K, Gohji K, Arakawa S, and Kamidono S. Elevation of serum levels of urokinase-type plasminogen activator and its receptor is associated with disease progression and prognosis in patients with prostate cancer. *Prostate*. 1999;39(2):123-9.
- Dohn LH, Illemann M, Hoyer-Hansen G, Christensen IJ, Hostmark J, Litlekalsoy J, von der Maase H, Pappot H, and Laerum OD. Urokinase-type plasminogen activator receptor (uPAR) expression is associated with T-stage and survival in urothelial carcinoma of the bladder. *Urologic oncology*. 2015.
- Kriegbaum MC, Persson M, Haldager L, Alpizar-Alpizar W, Jacobsen B, Gardsvoll H, Kjaer A, and Ploug M. Rational targeting of the urokinase receptor (uPAR): development of antagonists and non-invasive imaging probes. *Curr Drug Targets*. 2011;12(12):1711-28.
- Li D, Liu S, Shan H, Conti P, and Li Z. Urokinase plasminogen activator receptor (uPAR) targeted nuclear imaging and radionuclide therapy. *Theranostics*. 2013;3(7):507-15.
- Hanahan D, and Weinberg RA. The hallmarks of cancer. *Cell*. 2000;100(1):57-70.
- Ploug M, Ostergaard S, Gardsvoll H, Kovalski K, Holst-Hansen C, Holm A, Ossowski L, and Dano K. Peptide-derived antagonists of the urokinase receptor. affinity maturation by combinatorial chemistry, identification of functional epitopes, and inhibitory effect on cancer cell intravasation. *Biochemistry*. 2001;40(40):12157-68.
- Li ZB, Niu G, Wang H, He L, Yang L, Ploug M, and Chen X. Imaging of urokinase-type plasminogen activator receptor expression using a ⁶⁴Cu-labeled linear peptide antagonist by microPET. *Clinical cancer research: an official journal of the American Association for Cancer Research*. 2008;14(15):4758-66.
- Persson M, Madsen J, Ostergaard S, Jensen MM, Jorgensen JT, Juhl K, Lehmann C, Ploug M, and Kjaer A. Quantitative PET of human urokinase-type plasminogen activator receptor with ⁶⁴Cu-DOTA-AE105: implications for visualizing cancer invasion. *J Nucl Med*. 2012;53(1):138-45.
- Persson M HM, Madsen J, Jorgensen TJD, Jensen KJ, Kjaer A, Ploug M. Improved PET Imaging of uPAR Expression Using new ⁶⁴Cu-labeled Cross-Bridged Peptide Ligands: Comparative in vitro and in vivo Studies. *Theranostics*. 2013;3(9):618-32.
- Persson M, El Ali HH, Binderup T, Pfeifer A, Madsen J, Rasmussen P, and Kjaer A. Dosimetry of ⁶⁴Cu-DOTA-AE105, a PET tracer for uPAR imaging. *Nucl Med Biol*. 2014;41(3):290-5.
- Agency EM. *Guideline EMA/CPMP/ICH/286/1995*. EMA; 2009.
- Dano K, Andreasen PA, Grondahl-Hansen J, Kristensen P, Nielsen LS, and Skriver L. Plasminogen activators, tissue degradation, and cancer. *Advances in cancer research*. 1985;44:139-266.
- Yang Y, Adelstein SJ, and Kassis AI. General approach to identifying potential targets for cancer imaging by integrated bioinformatics analysis of publicly available genomic profiles. *Mol Imaging*. 2011;10(2):123-34.
- Sah BR, Burger IA, Schibli R, Friebe M, Dinkelborg L, Graham K, Borkowski S, Bacher-Stier C, Valencia R, Srinivasan A, et al. Dosimetry and First Clinical Evaluation of the New 18F-Radiolabeled Bombesin Analogue BAY 864367 in Patients with Prostate Cancer. *J Nucl Med*. 2015;56(3):372-8.
- DeIoar HM, Fujiwara T, Shidahara M, Nakamura T, Watabe H, Narita Y, Itoh M, Miyake M, and Watanuki S. Estimation of absorbed dose for

- 2-[F-18]fluoro-2-deoxy-D-glucose using whole-body positron emission tomography and magnetic resonance imaging. *European journal of nuclear medicine*. 1998;25(6):565-74.
32. Deloar HM, Fujiwara T, Shidahara M, Nakamura T, Yamadera A, and Itoh M. Internal absorbed dose estimation by a TLD method for 18F-FDG and comparison with the dose estimates from whole body PET. *Physics in medicine and biology*. 1999;44(2):595-606.
33. Anderson CJ, Dehdashti F, Cutler PD, Schwarz SW, Laforest R, Bass LA, Lewis JS, and McCarthy DW. ⁶⁴Cu-TETA-octreotide as a PET imaging agent for patients with neuroendocrine tumors. *J Nucl Med*. 2001;42(2):213-21.
34. Lewis JS, Laforest R, Dehdashti F, Grigsby PW, Welch MJ, and Siegel BA. An imaging comparison of ⁶⁴Cu-ATSM and ⁶⁰Cu-ATSM in cancer of the uterine cervix. *J Nucl Med*. 2008;49(7):1177-82.
35. Pfeifer A, Knigge U, Mortensen J, Oturai P, Berthelsen AK, Loft A, Binderup T, Rasmussen P, Elema D, Klausen TL, et al. Clinical PET of Neuroendocrine Tumors Using ⁶⁴Cu-DOTATATE: First-in-Humans Study. *J Nucl Med*. 2012;53(8):1207-15.
36. Tamura K, Kurihara H, Yonemori K, Tsuda H, Suzuki J, Kono Y, Honda N, Kodaira M, Yamamoto H, Yunokawa M, et al. ⁶⁴Cu-DOTA-trastuzumab PET imaging in patients with HER2-positive breast cancer. *J Nucl Med*. 2013;54(11):1869-75.
37. Wieser G, Mansi R, Grosu AL, Schultze-Seemann W, Dumont-Walter RA, Meyer PT, Maecke HR, Reubi JC, and Weber WA. Positron emission tomography (PET) imaging of prostate cancer with a gastrin releasing peptide receptor antagonist—from mice to men. *Theranostics*. 2014;4(4):412-9.
38. Boswell CA, Sun X, Niu W, Weisman GR, Wong EH, Rheingold AL, and Anderson CJ. Comparative in vivo stability of copper-64-labeled cross-bridged and conventional tetraazamacrocyclic complexes. *J Med Chem*. 2004;47(6):1465-74.
39. Jones-Wilson TM, Deal KA, Anderson CJ, McCarthy DW, Kovacs Z, Motekaitis RJ, Sherry AD, Martell AE, and Welch MJ. The in vivo behavior of copper-64-labeled azamacrocyclic complexes. *Nucl Med Biol*. 1998;25(6):523-30.
40. Ferdani R, Stigers DJ, Fiamengo AL, Wei L, Li BT, Golen JA, Rheingold AL, Weisman GR, Wong EH, and Anderson CJ. Synthesis, Cu(II) complexation, ⁶⁴Cu-labeling and biological evaluation of cross-bridged cyclam chelators with phosphonate pendant arms. *Dalton Trans*. 2012;41(7):1938-50.
41. Stigers DJ, Ferdani R, Weisman GR, Wong EH, Anderson CJ, Golen JA, Moore C, and Rheingold AL. A new phosphonate pendant-armed cross-bridged tetraamine chelator accelerates copper(ii) binding for radiopharmaceutical applications. *Dalton Trans*. 2010;39(7):1699-701.
42. Anderson CJ, Wadas TJ, Wong EH, and Weisman GR. Cross-bridged macrocyclic chelators for stable complexation of copper radionuclides for PET imaging. *Q J Nucl Med Mol Imaging*. 2008;52(2):185-92.
43. Sprague JE, Peng Y, Fiamengo AL, Woodin KS, Southwick EA, Weisman GR, Wong EH, Golen JA, Rheingold AL, and Anderson CJ. Synthesis, characterization and in vivo studies of Cu(II)-64-labeled cross-bridged tetraazamacrocyclic-amide complexes as models of peptide conjugate imaging agents. *J Med Chem*. 2007;50(10):2527-35.
44. Wong EH, Weisman GR, Hill DC, Reed DP, Rogers ME, Condon JS, Fagan MA, Calabrese JC, Lam KC, Guzei IA, et al. Synthesis and characterization of cross-bridged cyclams and pendant-armed derivatives and structural studies of their copper(II) complexes. *J Am Chem Soc*. 2000;122(43):10561-72.
45. Guo Y, Ferdani R, and Anderson CJ. Preparation and biological evaluation of (⁶⁴cu labeled tyr(3)-octreotate using a phosphonic Acid-based cross-bridged macrocyclic chelator. *Bioconjug Chem*. 2012;23(7):1470-7.
46. Wei L, Ye Y, Wadas TJ, Lewis JS, Welch MJ, Achilefu S, and Anderson CJ. (⁶⁴Cu)-labeled CB-TE2A and diamsar-conjugated RGD peptide analogs for targeting angiogenesis: comparison of their biological activity. *Nucl Med Biol*. 2009;36(3):277-85.
47. Wadas TJ, Eiblmaier M, Zheleznyak A, Sherman CD, Ferdani R, Liang K, Achilefu S, and Anderson CJ. Preparation and biological evaluation of ⁶⁴Cu-CB-TE2A-sst2-ANT, a somatostatin antagonist for PET imaging of somatostatin receptor-positive tumors. *J Nucl Med*. 2008;49(11):1819-27.
48. Szekanecz Z, Haines GK, and Koch AE. Differential expression of the urokinase receptor (CD87) in arthritic and normal synovial tissues. *Journal of clinical pathology*. 1997;50(4):314-9.
49. Ronday HK, Smits HH, Van Muijen GN, Pruszczynski MS, Dolhain RJ, Van Langelaan EJ, Breedveld FC, and Verheijen JH. Difference in expression of the plasminogen activation system in synovial tissue of patients with rheumatoid arthritis and osteoarthritis. *British journal of rheumatology*. 1996;35(5):416-23.
50. Fuhrman B. The urokinase system in the pathogenesis of atherosclerosis. *Atherosclerosis*. 2012;222(1):8-14.
51. Svensson PA, Olson FJ, Hagg DA, Ryndel M, Wiklund O, Karlstrom L, Hulthe J, Carlsson LM, and Fagerberg B. Urokinase-type plasminogen activator receptor is associated with macrophages and plaque rupture in symptomatic carotid atherosclerosis. *International journal of molecular medicine*. 2008;22(4):459-64.
52. Cermik TF, Mavi A, Basu S, and Alavi A. Impact of FDG PET on the preoperative staging of newly diagnosed breast cancer. *Eur J Nucl Med Mol Imaging*. 2008;35(3):475-83.
53. Siggelkow W, Rath W, Buell U, and Zimny M. FDG PET and tumour markers in the diagnosis of recurrent and metastatic breast cancer. *Eur J Nucl Med Mol Imaging*. 2004;31 (Suppl 1):S118-24.
54. Loeb S, Bjurlin MA, Nicholson J, Tammela TL, Penson DF, Carter HB, Carroll P, and Etzioni R. Overdiagnosis and overtreatment of prostate cancer. *Eur Urol*. 2014;65(6):1046-55.
55. Hansen HD, Ettrup A, Herth MM, Dyssegaard A, Ratner C, Gillings N, and Knudsen GM. Direct comparison of [(18) F]MH.MZ and [(18) F] altanserin for 5-HT2A receptor imaging with PET. *Synapse*. 2013;67(6):328-37.
56. Gillings N. A restricted access material for rapid analysis of [(11)C]-labeled radiopharmaceuticals and their metabolites in plasma. *Nucl Med Biol*. 2009;36(8):961-5.
57. Thurison T, Christensen IJ, Lund IK, Nielsen HJ, and Hoyer-Hansen G. Circulating intact and cleaved forms of the urokinase-type plasminogen activator receptor: biological variation, reference intervals and clinical useful cut-points. *Clin Chim Acta*. 2015;439:84-90.